Journal of Theoretical Biology 320 (2013) 159–169

Contents lists available at SciVerse ScienceDirect

Journal of Theoretical Biology

journal homepage: www.elsevier.com/locate/yjtbi

A predictive mathematical model of the DNA damage G2 checkpoint

Kevin J. Kesseler [a], Michael L. Blinov [b], Timothy C. Elston [c], William K. Kaufmann [a], Dennis A. Simpson [a,*]

[a] Department of Pathology and Laboratory Medicine, Lineberger Comprehensive Cancer Center, Center for Environmental Health and Susceptibility, University of North Carolina at Chapel Hill, NC 27599-7255, USA
[b] Center for Cell Analysis and Modeling, University of Connecticut Health Center, 263 Farmington Avenue, Farmington, CT 06030-1507, USA
[c] Department of Pharmacology, University of North Carolina at Chapel Hill,Chapel Hill, NC 27599-7260, USA

HIGHLIGHTS

- Predictive model of the transition from G2 phase of the cell cycle into mitosis.
- Includes protein phosphorylation sites, locations, concentrations, and activities.
- BioNetGen modeling approach to deal with large number of species and reactions.
- Extensively validated against both published studies and new experimental evidence.
- Likely to provide insight into the design of targeted cancer drugs.

ARTICLE INFO

Article history:
Received 21 May 2012
Received in revised form
21 November 2012
Accepted 10 December 2012
Available online 22 December 2012

Keyword:
Cell cycle

ABSTRACT

A predictive mathematical model of the transition from the G2 phase in the cell cycle to mitosis (M) was constructed from the known interactions of the proteins that are thought to play significant roles in the G2 to M transition as well as the DNA damage- induced G2 checkpoint. The model simulates the accumulation of active cyclin B1/Cdk1 (MPF) complexes in the nucleus to activate mitosis, the inhibition of this process by DNA damage, and transport of component proteins between cytoplasm and nucleus. Interactions in the model are based on activities of individual phospho-epitopes and binding sites of proteins involved in G2/M. Because tracking phosphoforms leads to combinatorial explosion, we employ a rule-based approach using the BioNetGen software. The model was used to determine the effects of depletion or over-expression of selected proteins involved in the regulation of the G2 to M transition in the presence and absence of DNA damage. Depletion of Plk1 delayed mitotic entry and recovery from the DNA damage-induced G2 arrest and over-expression of MPF attenuated the DNA damage-induced G2 delay. The model recapitulates the G2 delay observed in the biological response to varying levels of a DNA damage signal. The model produced the novel prediction that depletion of pkMyt1 results in an abnormal biological state in which G2 cells with DNA damage accumulate inactive nuclear MPF. Such a detailed model may prove useful for predicting DNA damage G2 checkpoint function in cancer and, therefore, sensitivity to cancer therapy.

Published by Elsevier Ltd.

1. Introduction

During the G2 phase of the cell cycle, preparations are made for the transition to mitosis. G2 is the final phase of the cycle where DNA damage can be repaired prior to mitotic cell division (Stark and Taylor, 2006). In response to DNA damage, either endogenous or exogenous, the DNA damage G2 checkpoint pathway is activated. By delaying entry into mitosis and helping to coordinate DNA repair, it plays an important role in protecting cells against genetic alterations that may be involved in tumorigenesis. Attenuation of the DNA damage G2 checkpoint response has been reported in familial cancer syndromes (Hartwell and Kastan, 1994) and cancer (Kaufmann et al., 2008). Several reviews have discussed the G2 to M transition and the G2 checkpoint response to DNA damage (Abraham, 2001; Hutchins and Clarke, 2004; Niida and Nakanishi, 2006; Nilsson and Hoffmann, 2000; van Vugt and Medema, 2005). A consensus diagrammatic description has been developed (Harper and Elledge, 2007), including signaling from the DNA damage sensor checkpoint kinases ATM and ATR to transducer checkpoint kinases Chk1 and Chk2, which act to inhibit cyclin B1/Cdk1 (MPF) kinase activity and exclude MPF from the nucleus, thereby delaying mitotic entry. Since DNA damage G2 checkpoint function may protect against cell killing by radio- and chemotherapies used for cancer, it would be valuable to predict checkpoint function before

* Corresponding author. Tel.: +1 919 966 8552.
E-mail address: dsimpson@med.unc.edu (D.A. Simpson).

0022-5193/$ - see front matter Published by Elsevier Ltd.
http://dx.doi.org/10.1016/j.jtbi.2012.12.011

therapy is initiated. Defects in DNA damage checkpoint function have been identified in cancer cell lines (Doherty et al., 2003; Kaufmann et al., 2008). Given the complexity of the interactions among the components of the G2-M transition and the DNA damage G2 checkpoint, it is likely that variation in protein expression levels impacts G2 checkpoint function in cancer cells. Thus a computational model of the G2-M transition and DNA damage G2 checkpoint may be used to predict how variation in protein expression influences checkpoint function (Qu et al., 2003; Tyson et al., 2011). Drawing on the extensive and sometimes contradictory body of experimental evidence available, we have developed a novel computational model of the DNA damage G2 checkpoint. It includes interactions among 16 proteins located in two compartments, their complexes and multiple phosphoforms, described by a set of 138 rules on conditions on complex formation and activities of multiple phosphorylation sites. When fully extended, the reaction network includes 769 species and 2688 reactions. However, the rule-based approach we use allows us to seamlessly manipulate such a large model, testing variable hypothesis, drug effects and parameter variability.

The model is centered on two positive feedback loops: the mutual activation of MPF and Cdc25c and the mutual inhibition of MPF and Wee1. The resulting system exhibits hysteresis, which has also been observed experimentally (Pomerening et al., 2003; Sha et al., 2003). It differs significantly from other G2 checkpoint and cell cycle models (Aguda, 1999; Novak et al., 1998) in including phosphorylation sites as well as nuclear and cytoplasmic compartments. While previous models have included phosphorylation sites (Gerard and Goldbeter, 2009) and compartments (Yang et al., 2006), this model is the first to incorporate both and is substantially more complex than these predecessors. It allows for the determination of whether or not the known reactions are sufficient to account for the experimentally observed behavior of the checkpoint or if additional unknown reactions are required. The compartmentalization of the model allows the investigation of the effects of nuclear import and export on checkpoint function. Furthermore, the model enables the rapid simulation of novel experimental conditions to guide future investigations. Lastly the model allows for the simulation of experiments that, with currently available techniques, are difficult or impossible to carry out at the bench such as experiments to deplete a given protein while altering the activity of another to simulate conditions that may be seen in some cancers or after exposure to a hypothetical agent. This modeling effort provides a platform for conducting in-silico experiments on G2 checkpoint function for both normal human cells as well as cancer cell lines. These types of simulations can be used to help guide experimental investigation as well as verify that our understanding of the protein-protein interactions underlying the G2 to M transition and G2 arrest mechanism is correct. The model not only recapitulates the published behaviors of the G2 to M transition and DNA damage G2 checkpoint (Rieder, 2011; van Vugt and Yaffe, 2010; van Vugt et al., 2010) but also predicts a novel regulation of intracellular trafficking of MPF that requires pkMyt1.

2. Model

2.1. Core model

The modeling of the DNA damage G2 checkpoint was begun by creating a model of the "core" of the checkpoint—the G2 to M transition. The core model is built around two positive feedback loops, a mutual activation loop consisting of MPF (it is assumed for the purpose of this model that CDK1 and cyclin B1 are always found in their bound state) and Cdc25 and a mutual inhibition loop consisting of MPF and Wee1. We assume that substrate and enzyme bind in a reversible reaction to form a complex and that the phosphatase or kinase activity of the enzyme occurs at a rate proportional to the concentration of the complex resulting in the dissociation of the complex.

$$[E]+[S]\leftrightarrow[ES]\rightarrow[E]+[P]$$

The activation of Wee1 and the deactivation of Cdc25 occur spontaneously at a rate proportional to the concentrations of inactive Wee1 and active Cdc25, respectively. As the total amount of Cdc25 is varied, the concentration of active MPF after equilibration switches from a low level to a high level (or vice versa). For appropriate choices of the rate constants this results in a bistable switch—a type of hysteresis where the equilibrium behavior of the system depends on the initial activity level of MPF in addition to the total amounts of the proteins (this bistable behavior is shown in Fig. 1). In a normal G2 to M transition the system will start with low levels of MPF and Cdc25 and a high level of active Wee1. This will result in the immediate deactivation of newly created MPF thus causing the switching to occur at the concentration of Cdc25 determined by the lower curve. The switching behavior demonstrated by this model represents the basic dynamics of the G2-M transition (Novak et al., 2007, 2010).

2.2. Extended model

The core model was extended to include 16 proteins in two compartments, the nucleus and the cytoplasm. The G2 to M

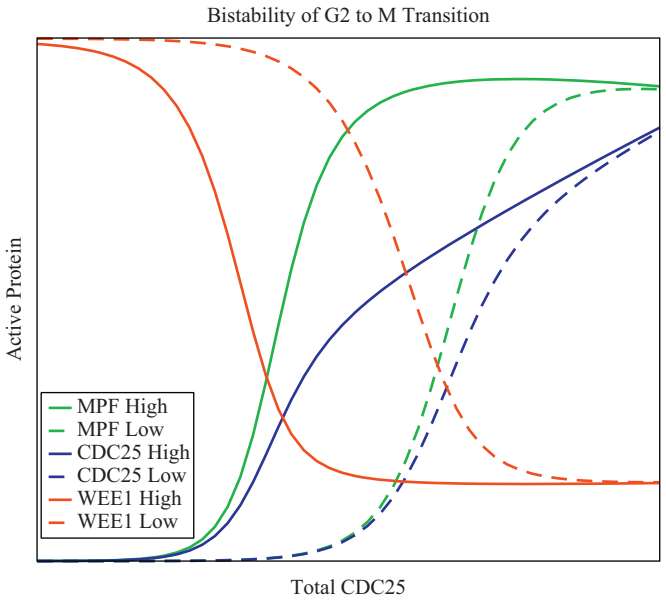

Fig. 1. Bistability of MPF activity in the model during the G2 to M Transition. This figure demonstrates the hysteresis in the core model of the DNA damage G2 checkpoint. The model consists of two positive feedback loops and three proteins: the mutual inhibition of MPF and Wee1 and the mutual activation of Cdc25 and MPF. For a given amount of the signal protein (Cdc25), the equilibrium concentration of the active form of the response protein (MPF) depends on the initial state of the system—in particular, if the MPF was mainly active or mainly inactive at the beginning of the simulation. The solid curves in the figure depict the results of simulations with MPF initially active and the dashed curves represent simulations where MPF was inactive at the outset. The red curves show equilibrium concentrations of active Wee1, the blue curves the amount of active Cdc25, and the green curves show the equilibrium value of active MPF. The total amount of Cdc25 present in the simulation increases along the positive *x*-axis. (For interpretation of the references to color in this figure legend, the reader is referred to the web version of this article.)

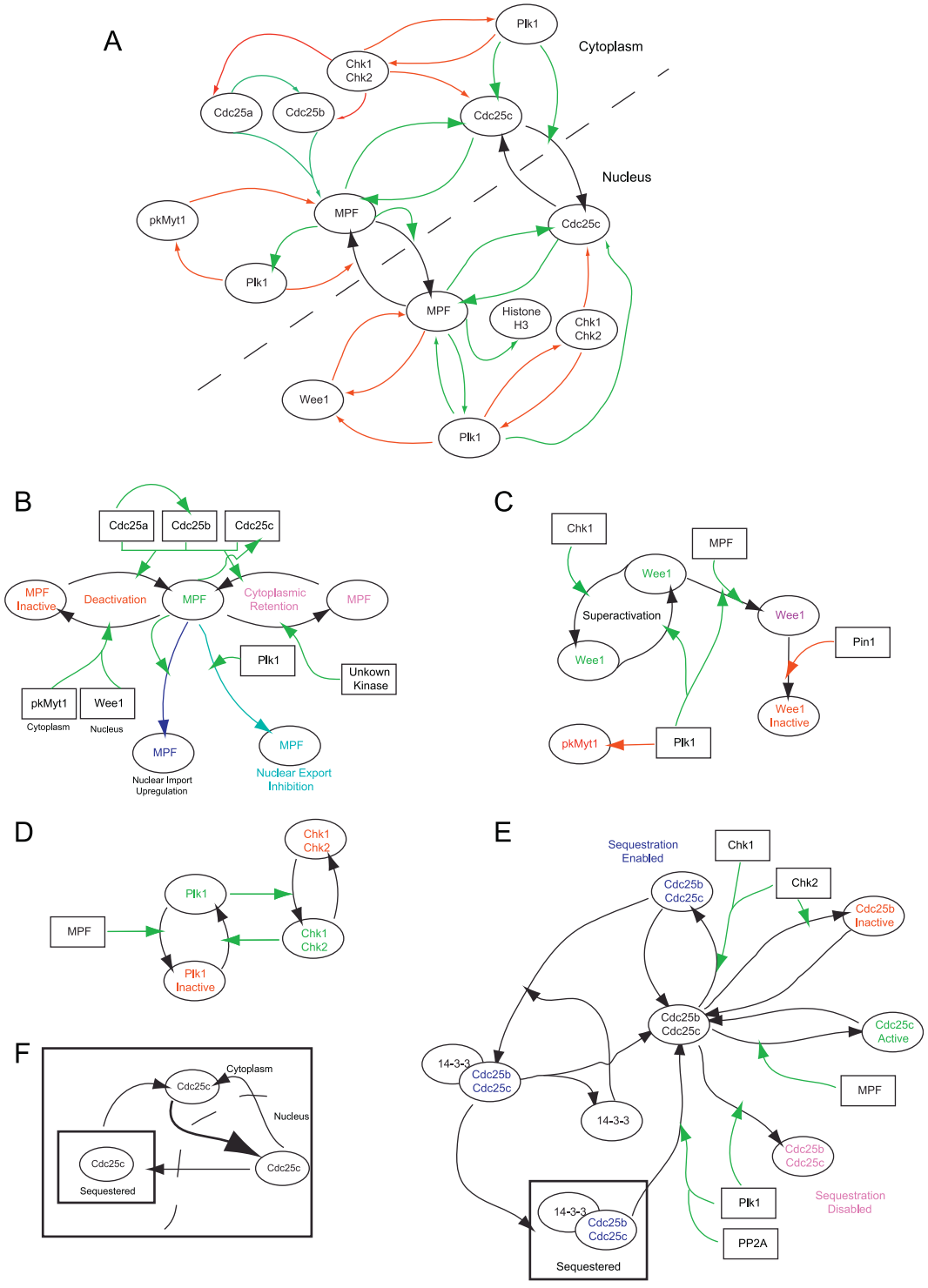

Fig. 2. Wiring Diagram of Reactants in the G2 checkpoint model. Panel (A) is a wiring diagram of the DNA damage G2 checkpoint showing the main proteins involved. Black arrows indicate transport, green arrows indicate up-regulation, and red lines indicate inhibition. Panel (B) shows a schematic of the reactions undergone by MPF in the model and the proteins mediating these reactions. Black arrows indicate change between different states of the proteins and green arrows indicate up-regulation. The possible states of MPF are represented by the colors green (active), red (deactivated due to phosphorylation by pkMyt1 or Wee1), purple (cytoplasmic retention phosphorylation), cyan (nuclear export inhibited by Plk1), and blue (nuclear import upregulated via autophosphorylation). Panel (C) is a schematic showing the regulation of pkMyt1 and Wee1. Black arrows indicate change between different states of the proteins (active [green], inactive [red], and tagged for deactivation [purple]). Green arrows indicate up-regulation, and red arrows indicate down-regulation. Panel (D) is a schematic showing the regulation of Plk1, Chk1, and Chk2. Black arrows represent transitions between active (green) and inactive (red) forms. Green arrows represent upregulation. Panel (E) shows a schematic of the reactions undergone by Cdc25b and Cdc25c in the model and the proteins mediating these reactions. Black arrows indicate a change between different states of the proteins and green arrows indicate up-regulation. Blue indicates that sequestration has been enabled by phosphorylation, red lettering represents inactive protein, green lettering indicates active protein, and purple lettering indicates that sequestration has been disabled due to phosphorylation by Plk1. Panel (F) demonstrates the transport of Cdc25c between the cytoplasm and nucleus. (For interpretation of the references to color in this figure legend, the reader is referred to the web version of this article.)

transition involves the proteins MPF, Cdc25a, Cdc25b, Cdc25c, Wee1, pkMyt1, PP2A, PIN1, Plk1, and an unidentified cytosolic kinase responsible for the phosphorylation on MPF to enforce cytoplasmic retention (CR). The DNA damage transducer kinases Chk1 and Chk2 activate the G2 arrest mechanism in the presence of a DNA damage signal. A 14-3-3 protein allows sequestration of the Cdc25's following Chk1 and Chk2. The intracellular locations of the proteins are regulated through importin (nuclear import) and Crm1 (nuclear export). Histone-H3 is included in the model as a marker of mitosis which is defined as 20% of the histone-H3 being phosphorylated by active MPF.

An overview of the model showing the nuclear and cytoplasmic compartments is illustrated in Fig. 2A and the interactions and transport of the various proteins are depicted in more detail in Fig. 2B–F. The regulation of MPF is shown in Fig. 2B. MPF is created in its active state in the cytoplasm and MPF is degraded at a constant rate in all states and locations. There is a negligibly low amount of MPF initially, thus the level of MPF rises until reaching a steady state. MPF is deactivated via phosphorylation by pkMyt1 in the cytoplasm or Wee1 in the nucleus.

Fig. 2C demonstrates the regulation of pkMyt1 and Wee1. The nuclear kinase Wee1, which deactivates MPF, may be phosphorylated by the active form of MPF or Plk1 after which its kinase activity may be permanently destroyed by the action of PIN1. MPF can also be deactivated by pkMyt1, which is located in the cytoplasm. pkMyt1 is down-regulated by the active form

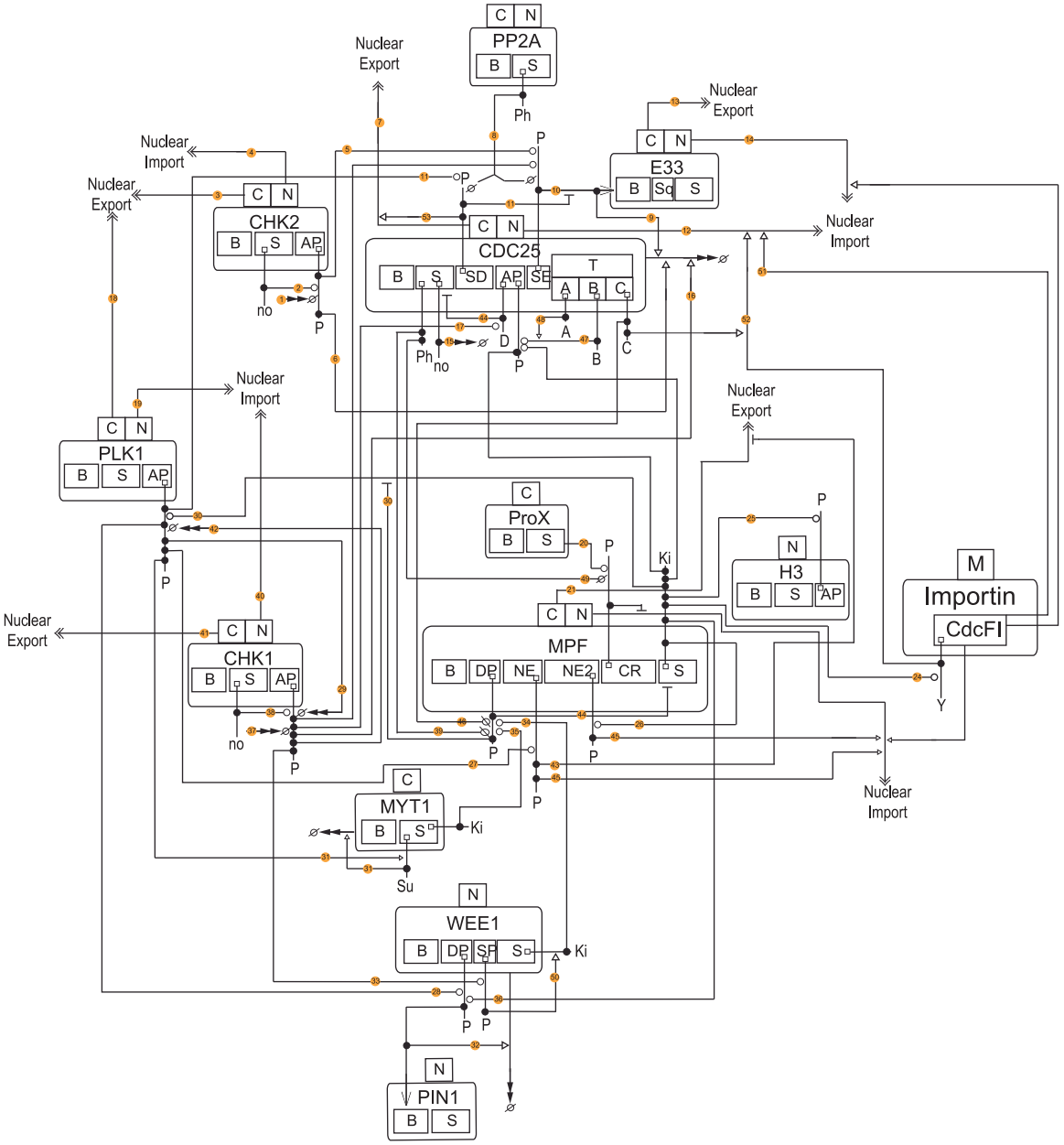

Fig. 3. Extended Contact Map (ECM) representing reactions found in the model. This ECM is drawn from the model rules following published guidelines (Chylek et al., 2011). The symbols used are a subset of those in Chylek et al. with the exception of the intracellular transport symbol. ●— Dependent reaction; —| Inhibition; —▷ Activation reaction; —» Multistep intracellular transport; ⊘ Catalysis, cleavage; —→ Multistep process; —◯ Covalent bond formation; —> Complex formation; ● Number in the colored circles correspond to note numbers in supplemental Table S2.

of Plk1. The regulation of Plk1 and Chk1/2 is shown in Fig. 2D. Plk1 and Chk1/2 mutually inhibit each other and Plk1 is activated by MPF (Chk1 and Chk2 are activated by a DNA damage signal).

The action of Wee1 is significantly enhanced via super-activation of Wee1 by Chk1 (Fig. 2C). The deactivating phosphorylations on MPF can be removed by the actions of Cdc25b or Cdc25c. MPF phosphorylates Wee1 which allows nuclear protein PIN1 to permanently destroy the kinase activity of Wee1 (which for the purposes of the model is effectively the same as destroying Wee1), as shown in Fig. 2C. The location of MPF is controlled by phosphorylations for cytoplasmic retention (CR) and nuclear export inhibition (NEI). Both PIN1 and unknown CR kinase remain at a constant level throughout. The CR phosphorylation is removed by Cdc25b/c. While there is no experimental evidence that Cdc25b/c performs this function it is reasonable to assume that such dephosphorylation will be carried out by a phosphatase with a similar activation profile as Cdc25b/c. The NEI phosphorylation may be put on by Plk1 or by MPF autophosphorylation of. The CR phosphorylation prevents MPF from being transported into the nucleus and the NEI phosphorylation greatly slows the rate of nuclear export of MPF. Thus, the states of these two phosphorylations determine where MPF is located. As shown in Fig. 2D, the activity of Plk1 is down-regulated by Chk1, which keeps Plk1 inactive when a damage signal is present, and up-regulated by MPF. Additionally, Plk1 also down-regulates Chk1 activity. These effects amplify the positive feedback of MPF activation, allowing for recovery from a G2 arrest.

As we mentioned, the model includes activities of multiple phosphorylation sites of proteins. MPF has several phosphorylation sites that are considered in this model. While pkMyt1 phosphorylates T14 and Y15 and Wee1 only phosphorylates Y15, both effectively deactivate MPF and both phosphorylations are removed by Cdc25b/c. For this reason T14 and Y15 are represented as a single phosphorylation site in the model. The other phosphorylation sites in the model are involved in regulating nuclear import and export. The CR phosphorylation prevents the import of MPF into the nucleus, thus keeping it in the cytoplasm. It is known that three additional sites promote preferential import into the nucleus (modeled by fast import and slow export). Two of these sites are auto-phosphorylated by MPF and the other one is phosphorylated by Plk1. It is assumed that the effects of these phosphorylations are equivalent and, for that reason, these three different phosphorylations are not distinguished in the model and are modeled as a single site.

The model uses a single molecular entity to represent all three CDC25's found in mammalian cells. This entity has a marker designating it as CDC25a, b, or c (Fig. 3). Regulation of Cdc25b/c is shown in Fig. 2E. Cdc25b is localized in the cytoplasm while Cdc25c is present in both the nucleus and the cytoplasm (a schematic of the transport of Cdc25c is shown in Fig. 2F). Both forms of Cdc25 behave the same with regard to sequestration; Phosphorylation by Chk1 or Chk2 at S216 allows 14-3-3 protein to bind to the Cdc25b/c, after which the complex of Cdc25b/c and 14-3-3 is sequestered in the cytoplasm. The Cdc25b/c can be removed from sequestration by the action of PP2A or Plk1, both of which free the complex and dissociate it. This is the primary mechanism for G2 arrest, lowering the available Cdc25b/c thus preventing positive feedback from activating MPF. Additionally, Plk1 can phosphorylate Cdc25b/c and prevent 14-3-3 binding and sequestration.

The model does not contain the numerous pathways that regulate the stability and activation of CDC25b in vivo. To approximate the synthesis and degradation of Cdc25b in the model it is produced in its inactive form in the cytoplasm and degrades in all states. It is activated by Cdc25a as well as spontaneously and is deactivated via phosphorylation by Chk1, thus suppressing Cdc25b function when a damage signal is present. Cdc25b behaves the same as Cdc25c with respect to sequestration by 14-3-3 and the related phosphorylations by Chk1, Chk2, and Plk1.

Cdc25b activity begins the activation of the cytoplasmic MPF (as well as the removal of the CR phosphorylation) then MPF is transported into the nucleus (where most of it remains due to the NEI phosphorylation) and the positive feedback between Cdc25c and MPF causes the rapid expansion of active MPF, which sends the cell into mitosis.

As Cdc25c is produced in its inactive form and rapidly transported to the nucleus, the model assumes that it is created inactive in the nucleus. While Cdc25c can be cytoplasmic, preferential nuclear import causes the bulk of (unsequestered) Cdc25c to be located in the nucleus, although it may be moved into sequestration in the cytoplasm. Cdc25c is activated by MPF and deactivates spontaneously. Like MPF, it degrades at a constant rate in all states and locations. Like Cdc25b it can be phosphorylated at ser216 by Chk1 or Chk2, allowing 14-3-3 to bind, after which the complex is sequestered in the cytoplasm. Cdc25c also has a site that Plk1 can phosphorylate, which prevents binding and sequestration by 14-3-3 (Toyoshima-Morimoto et al., 2002).

2.3. Modeling methods

The model includes 769 distinct molecular species comprising 16 proteins, their various complexes and phosphorylation forms, involved in 2688 reactions. The model includes only binary complexes of proteins; however, many of the proteins we consider are subject to post-translational modifications involving multiple sites, such as MPF and Cdc25 each having 4 sites subject to phosphorylation, with each site responsible for different behavior. Consideration of all of the potential phospho-forms of these proteins leads to explosion in the number of species, as a protein with 4 phospho-sites that can each be in two possible states yields $2^4=32$ potential phosphoforms, each of which is considered a distinct species in the model. Including complex formations based on interactions between binding sites of proteins resulting in 769 molecular species.

A computational model that describes interactions among chemical species typically includes an Ordinary Differential Equation (ODE) for each chemical species. Each ODE is comprised of mass-action terms for every reaction influencing the concentration of the molecular species corresponding with the ODE. To account for hundreds of species and thousands of interactions, one cannot use the approach of writing equations manually. Therefore, we used a rule-based approach (Blinov et al., 2004; Hlavacek et al., 2006) to generate the chemical reaction network (and corresponding system of ODEs). In this approach, chemical reactions are not written explicitly but are represented by rules. A rule specifies the features of reactants and products that are relevant for a type of reaction that can result from a particular protein–protein interaction, which is usually mediated by specific parts of the interacting proteins. Given a set of species, a rule identifies those species that have the features required to undergo the transformation from reactants to products specified in the rule. By convention, it is assumed that the interaction represented in a rule is independent of features not explicitly indicated. Thus, multiple species may qualify as reactants in a type of reaction defined by a rule.

The model is specified by 138 rules documented in the Extended Contact Map (ECM) shown in Fig. 3 and a commented code that can be found in the supplemental materials Table S2 (Chylek et al., 2011).

In Fig. 3, every arrow represents not a single reaction but a group of reaction rules that describe a class of reactions. For example, in the activation of MPF by Cdc25 by dephosphorylation the rule (note 39 in Fig. 3 and supplemental Table S2) only requires that Cdc25 has its activating phosphorylation and MPF has a deactivating phosphorylation. The state of two other phosphorylation sites on Cdc25 and three other sites on MPF are irrelevant to this rule resulting in the large number of reactions generated. A major assumption of rule-based modeling is that all reactions generated by a rule have the same rate laws. Although this assumption may not be true in general, rules are selected in such a way that variation in kinetics among reactions generated by the rule is less than the change in kinetics between different rules. For example, the rate of degradation of MPF protein is assumed to be independent of its phosphorylation states. The exact number of reactions generated by a rule depends, in general, on the entire set of rules in which the rule of interest is found and also on the set of species to which rules are initially applied. The class of interactions involved in the activation of MPF by Cdc25 (the first rule in group 39 of Table S2,

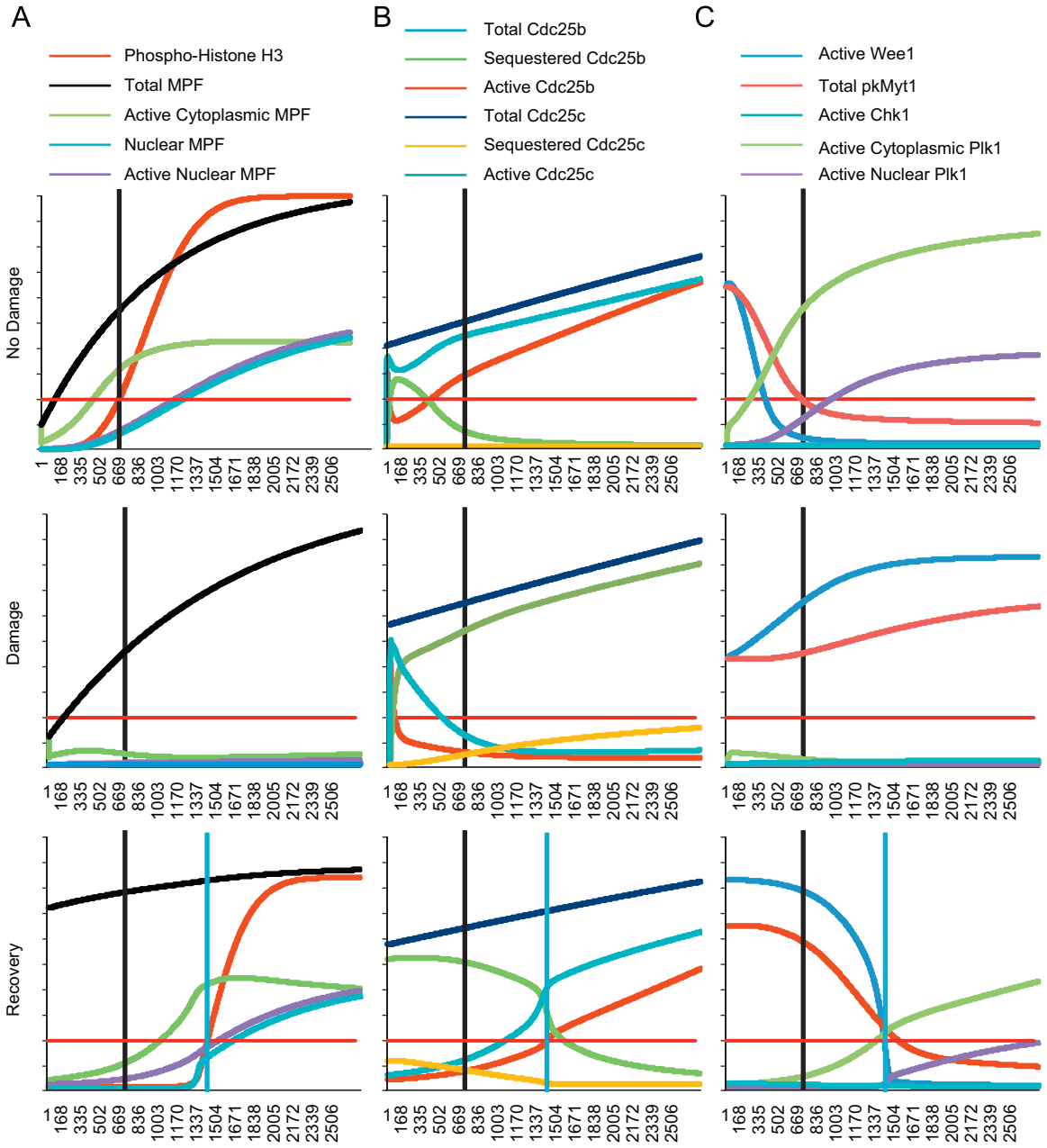

Fig. 4. Base model simulations. The *y*-axis is protein concentration and the x-axis is time step of model in arbitrary units. Each column shows concentration time courses for a particular group of protein species (see legend below) and each row shows results from one of three trial conditions: No Damage (top); Damage (middle); Recovery (bottom). The "No Damage" trial shows normal behavior with no DNA damage signal being sent; the "Damage" trial shows the behavior in response to a constant damage signal; and the "Recovery" trial shows the result of turning off the damage signal after an 8 h damage arrest. The red horizontal line in each panel indicates 20% of total concentration. Model entry into mitosis is indicated by the phosphor-histone H3 level reaching the 20% line (the red curve in the rightmost panels crossing the red line). The vertical line in each panel corresponds to the time step in which phosphor-histone H3 reaches 20% in the "No Damage" trial—this is defined to be 3 h. Column A: Phospho-Histone H3; Total MPF; Active Cytoplasmic MPF; Nuclear MPF; Active Nuclear MPF. Column B: Total Cdc25b; Sequestered Cdc25b; Active Cdc25b; Total Cdc25c; Sequestered Cdc25c; Active Cdc25c Column C: Active Wee1; Total Myt1; Active Chk1; Active Cytoplasmic Plk1; Active Nuclear Plk1. (For interpretation of the references to color in this figure legend, the reader is referred to the web version of this article.)

Table 1
Initial parameter settings for depletion experiments.

Experiment	Molecule(s)	Altered parameter values		Trial level[c] (%)
		Initial concentration	Synthesis rate	
pkMyt1 depletion Fig. 5a	pkMyt1	0.5	0.001	0
		0.005	0.00001	1
		0.05	0.0001	10
Wee1 depletion Fig. 5a	Wee1	0.5	0.005	0
		0.005	0.00005	1
		0.05	0.0005	10
pkMyt1 and Wee1 depletion Fig. 5a	pkMyt1	0.005	0.00001	1
	Wee1	0.005	0.00005	
	pkMyt1	0.05	0.0001	10
	Wee1	0.05	0.0005	
Plk1 depletion[a] Fig. 5b	Plk1	0 cyt 0 nuc	N/a	0
		0.007 cyt 0.003 nuc	N/a	1
		0.07 cyt 0.03 nuc	N/a	10
Plk1 depletion[b] pkMyt1 and Wee1 overexpression Fig. 5b	Plk1	0.07 cyt 0.03 nuc	N/a	10
	pkMyt1	2.5	0.005	500
	Wee1	2.5	0.025	
Plk1 depletion[b] Wee1 depletion Fig. 5c	Wee1	0.005	0.00005	1
		0.05	0.0005	10
Plk1 depletion[b] pkMyt1 depletion Fig. 5c	Plk1	0.005	0.00001	1
	pkMyt1	0.05	0.0001	10

[a] In the model there is a constant amount of Plk1, no synthesis or destruction. Since there is a constant amount of Plk1 in the model and it is not transported between compartments, it remains where it is seeded. Cytoplasmic=cyt and Nuclear=nuc.
[b] The Plk1 initial conditions were set to give 10% of baseline values of Plk1 as shown above.
[c] The amount of the targeted molecule at steady state as compared to the baseline value.

supplemental material) generates 192 reactions. The large number of reactions in this class is due to several phospho-sites on both MPF and Cdc25 that do not affect the activation of MPF. Rule application is iterative and halts when all possible reactions are generated. A biological model is specified using BioNetGen Language (BNGL) that encodes molecules, initial species, reaction rules and simulation parameters, and is simulated using BioNetGen software (Blinov et al., 2004; Colvin et al., 2009; Faeder et al., 2009)

2.4. Modeling rate constants

This model was constructed of protein–protein interactions and protein transport mechanisms that have been shown in the literature to play a role in the G2 to M transition or the DNA damage G2 checkpoint. Because of the large number of reactions in this model and a lack of experimental data to set protein levels and reaction rate constants, all of the proteins either have a constant expression level or are created and degraded at constant rates with an equilibrium level which is set to the non-dimensional value of 1 for convenience. The majority of the 135 rate constants in the model have not been measured experimentally, so they were chosen initially based on the relative speed of different reactions. The sequestration of Cdc25b/c by 14-3-3 requires a one-to-one correspondence between Cdc25b/c and 14-3-3. In this case, the total amount of Cdc25 which may be sequestered is limited by the amount of 14-3-3 available to bind to it. For the purposes of this model equal amounts of both proteins have been used. In order to be definitive, the time for the transition from the beginning of G2 to the beginning of mitosis is taken to be 3 h.

Due to the lack of experimentally determined rate constants and concentrations, it must be demonstrated that the observed behavior is not the result of a particular choice of parameters, but rather qualitatively consistent over a wide range of parameter values. In order to do this we have conducted a parameter study in which we generated a group of randomly perturbed parameter sets and ran the same series of simulations that we had run for our initial parameter set for each of the perturbations. These results were consistent with the results from the original parameter set. Specifically, we perturbed all rate constants in the model by multiplying each constant by a random factor from a uniform distribution on the interval [0.5, 1.5]. Some of the parameters were multiplied by the same random factor in order to preserve intentional relationships, i.e., rates for the same reaction in different compartments or groups of rates which were all intentionally set to the same value (such as the rate for complex dissolution or enzymatic activity in phosphatase and kinase reactions). 800 of these parameter sets were generated to ensure that the perturbations cover a reasonable part of the parameter space. The results of simulations run for all of these parameter sets are shown in Fig. S1.

3. Model validation

The model was validated by the numerical simulation of numerous experiments for which data was available or could be empirically obtained. Each experiment consisted of the same three trials described in the *Baseline Simulations* section below with the initial concentration and/or creation rate of one or more model proteins changed from their baseline values.

3.1. Baseline simulations

Multiple simulations were performed on the model in order to validate it. Each simulation corresponds to a numerical experiment on a different phenotype in the model (typically the depletion or over expression of one or more proteins). All runs start with the cessation of DNA synthesis and the inactivation of the Chk1-mediated replication checkpoint that prevents

mitosis until DNA replication is completed. Chk1 is active during DNA replication and completion of DNA replication allows Chk1 to be inactivated. The first type of run was a simulation showing the normal G2 to M progression in the absence of a damage signal. The runs of this type were started with 10% of CHK1 and CHK2 active and declined rapidly to a negligible amount. Histone H3, a nuclear target of MPF, was chosen to indicate entry into mitosis. In experiments, cells with detectable levels of phospho-histone H3 are committed to mitosis (Juan et al., 1998). A level of 20% histone H3 phosphorylation was chosen as indicative of entry into mitosis. The model uses arbitrary time units, so in order to relate the model to biological experiments we have chosen to equate the time to normal entry in the baseline case with the length of G2 in normal cells. In the baseline case 20% of histone H3 is phosphorylated after about 670 time units. In mammalian cells proliferating with a 24-h doubling time, the length of G2 phase of the cell is about 3 h. For this reason, the length of the time unit was chosen so that normal entry time in the baseline case represents 3 h.

The second type of experiment was a simulation of a DNA damage-induced arrest of the cell cycle. This can essentially be thought of as an experiment where a DNA damaging agent such as the topoisomerase II poison etoposide is added to the cell and never removed. In these runs active CHK1 and CHK2 increased from the initial low level until they were both fully activated and remained at the fully active level for the duration of the run. For all model simulations the DNA damage response was run for the equivalent of 12 h (2700 time steps). In the baseline case, the arrest can be sustained for over 20 h with less than 5% of the histone H3 phosphorylated (data not shown). The final experiment was a simulation of recovery from a damage arrest. In these simulations a damage arrest simulation is run for 8 h after which the damage signal is turned off causing the level of active CHK1 and CHK2 to decrease until both are inactive. In the baseline case for this type of run histone H3 phosphorylation reaches the 20% level about 3 h after the deactivation of the damage signal (Fig. 4).

3.2. Parameter perturbation study

To perform and analyze parameter perturbation, we write several scripts (described in the *Parameter Perturbation Study* section of the supplement legend file) that set up the BioNetGen language model files for each combination of parameter set, experiment, and trial; run the resulting simulation; determine the time of mitotic entry (if any) from the resulting data; and collate and process the results into the information displayed in the figures.

3.3. Wee1 and pkMyt1 depletion

Wee1 and pkMyt1 are negative regulators of MPF (Niida and Nakanishi, 2006; Wang et al., 2004; Wells et al., 1999). Loss of function of these kinases is predicted to attenuate the DNA damage G2 checkpoint (Wang et al., 2004). Studies utilizing inhibitors of Wee1 are being evaluated in early clinical trials for efficacy in reducing tumor size (Hirai et al., 2009). These inhibitors likely inhibit pkMyt1 to some degree as well. For these reasons it was of interest to simulate reduced Wee1 and pkMyt1 levels in the model. The initial parameter values for the starting concentration and synthesis rate for all the depletion studies is found in Table 1. Model simulations were run with Wee1 or pkMyt1 depleted to 0%, 1% and 10% of baseline levels as well as depleting both proteins to 1% or 10% of baseline. Depletion of Wee1 to any level resulted in a modest 18 min to 24 min reduction in the length of G2. However at the very low levels of Wee1 the cells were unable to sustain a checkpoint response (Fig. 5a). This contrasts with the pkMyt1 depletions where G2 is 30 min to 36 min shorter than the baseline case while all pkMyt1 depletions are able to sustain a checkpoint response (Fig. 5a). Although the pkMyt1-depleted cells are able to sustain a G2 checkpoint response, the recovery from the DNA damage is 3 h to 3.5 h faster than the baseline case. The double depletions have a severe effect on both the length of G2 and the ability to sustain a G2 checkpoint.

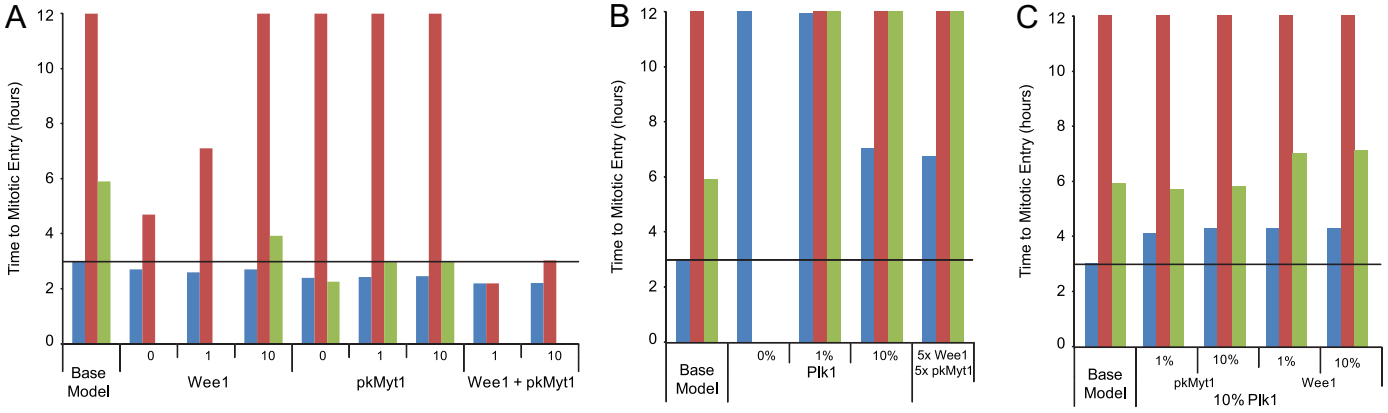

Fig. 5. Effects of reductions in Wee1, pkMyt1, or Plk1 proteins. The horizontal line in each panel marks the time point were the Base Model enters mitosis. This time step (675) was defined as representing 3 h for purposes of the figures. No Damage; Damage; Recovery. In the No Damage and Damage cases the simulations were run for 12 h (2700 time steps). To simulate Recovery from Damage the model was run for 8 h with damage (1789 time steps) followed by a simulated 12-h recovery time. In both panels the *X*-axis refers to the protein depleted and the numbers represent 0%, 1%, or 10% of the Base Model levels of the given protein. Panel (A) shows that a partial depletion of Wee1 (10% remaining) speeds up recovery of DNA damage while a more complete depletion attenuates the damage response. This is seen as cells entering mitosis with a DNA damage signal. The effects of depletion of pkMyt1 alone were more modest with the only effect seen was a faster recovery from the DNA damage response. Double depletions speed up mitotic entry and ablate the DNA damage response. Missing bars in the histogram are because cells went into mitosis during the DNA damage response. Panel (B) depicts a partial depletion of Plk1and shows a slowing of entry into mitosis and a block of recovery of the DNA damage response. The model is dependent on Plk1 for mitotic entry. Depletion of Plk1 in biological systems results in an increase in the amount of Wee1 and pkMyt1 in the cell. This condition was simulated by increasing the amount of Wee1 and pkMyt1 fivefold and decreasing the amount of Plk1 to 10% (5 × Wee1, 5 × pkMyt1). This did not alter the outcome suggesting that the mitotic delay and lack of recovery from DNA damage in the Plk1 depleted simulation is due entirely to Plk1 levels. Panel (C) is a histogram showing the results of a simulation depleting Plk1 to 10% of baseline combined with pkMyt1 depletions or Wee1 depletions. This simulation suggests that partial depletion of pkMyt1 or Wee1 can restore the DNA damage G2 checkpoint recovery lost in the Plk1 depleted cells. This is an example of an experiment that might not be performed at the bench without prior knowledge of the expected results due to the difficulty in controlling the depletion of the proteins.

3.4. Plk1 depletion

Simulations were conducted to determine the effects of Plk1 depletion on the model (Table 1, and Fig. 5b). In the model, complete loss of Plk1 blocks cells in G2. Plk1 at 1% of baseline levels is similar to complete loss of Plk1. Mitotic entry does not occur until 11.9 h. Plk1 at 10% of baseline approximately doubles the time required to enter mitosis and blocks the recovery from the DNA damage response.

In the model, depletion of Plk1 to 10% of baseline levels resulted in an over-expression of both pkMyt1 and Wee1. To further validate the model it was of interest to determine if this occurs experimentally following Plk1 depletion by RNAi in synchronized normal human fibroblasts. Fig. 5b shows that the experimental results are in good agreement with the simulation. The vertical lines on the graphs represent the point at which the cells enter mitosis. Since the amount of pkMyt1 and Wee1 appeared to have a greater fold increase in the experimental results than in the simulations, a simulation was conducted that increased the amount of pkMyt1 and Wee1 by fivefold while reducing the amount of Plk1 to 10% of baseline. This condition was not different than simply reducing the amount of Plk1 to 10% of baseline (Fig. 5b). To test the utility of simulating experiments that are difficult to perform at the bench, a simulation was run in which the amount of Plk1 was reduced to 10% of baseline and the amount of pkMyt1 or Wee1 was then varied (Table 1, and Fig. 5c). This simulation predicts that a reduction of pkMyt1 or Wee1 will rescue the inability of cells depleted for Plk1 to recover from a DNA damage induced G2 checkpoint.

3.5. Experimental model validation

Normal human fibroblasts were grown at 37 °C in MEM (Invitrogen) supplemented with non-essential amino acids (Invitrogen) and 10% Bovine Growth Serum (Hyclone). RNAi (non-targeting control and Plk1) were obtained from Dharmacon. Cells that were synchronized to G0 were electroporated with the Nucleofector II according to manufacture protocol U-23 (Lonza, Germany) using 80 pM RNAi per one million cells. Electroporated cells were stimulated to divide by plating at sub-confluent density then collected at the beginning of S phase by incubation with aphidicolin. Upon removal of aphidicolin from medium, cells synchronously progressed through S, G1 and M (Unsal-Kacmaz et al., 2005). Relative protein amounts were determined by pixel density from film. Antibodies for Western blot were obtained from Milli-Pore. Fig. 6 shows the results of this experiment as well as its simulation by the model. The results of the simulation are in good agreement with the biological results.

3.6. Plk1 and MPF over-expression

Altered expression of Plk1 and MPF is frequently observed in many cancers and has been shown to transform NIH3T3 cells (Takai et al., 2005; van Vugt and Medema, 2005). Additionally studies conducted with constitutively active Plk1 have shown that cells enter mitosis regardless of the presence of a damage signal (Smits et al., 2000). Taken together, these studies argue that the excess levels of Plk1 are likely leading to chromosomal instabilities possibly as a result of premature adaptation of the DNA damage checkpoint response. Since most cancers have lost p53 function, a negative regulator of MPF expression, it was of interest to model a series of simulations examining the over-expression of MPF and Plk1. In these simulations the total amount of Plk1 protein or the rate of MPF production were increased tenfold. An additional simulation was run in which all Plk1 was constitutively active. All three of these simulations resulted in a G2 phase of less than 2 h and no ability of the model to sustain a G2 checkpoint response for more than 2 h.

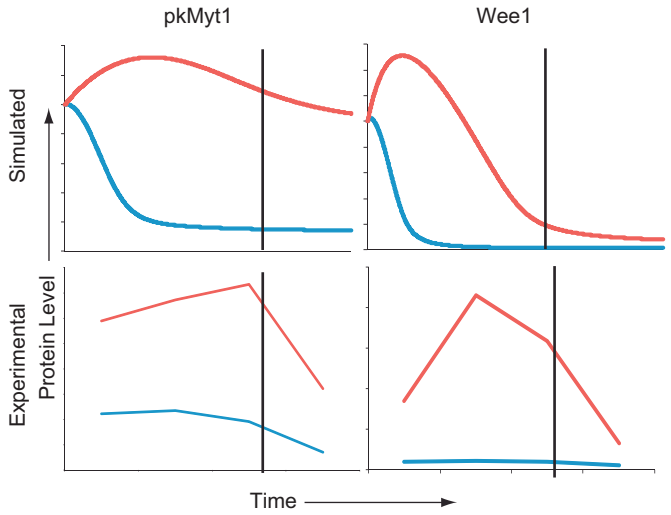

Fig. 6. Validation of model results with respect to amount of pkMyt1 or Wee1 present after depletion of Plk1. The upper two panels are the results from either a Base Model simulation or one in which the initial amount of Plk1 is reduced to 10% of the Base Model. The lower two panels are the results from an experiment with synchronized normal human fibroblasts where the amount of Plk1 was reduced by RNAi to approximately 10% of the control. The horizontal axis is time and the vertical axis is protein concentration. The vertical line in each panel shows mitotic entry. Non-Targeting Control siRNA or Base Model; Plk1 RNAi or 10% Plk1 in simulation. The amount of pkMyt1 or Wee1 present in the biological samples (lower panels) is in good agreement with the model simulations (upper panel).

3.7. Chk1 and Chk2 depletions

While the current version of the model does not contain the pathways that regulate Chk1 and Chk2, the activity levels of both are used for the checkpoint signal within the model. That this signal works in the model was explored by depleting either Chk1 or Chk2 to 0%, 1%, or 10% of the base level. Depletion of Chk1 to any of these levels resulted in an accelerated entry into mitosis (2 h vs. 3 h in baseline) and a model that could not sustain the G2 DNA damage checkpoint response for more than about 2 h (supplement Fig. S2). Depletion of Chk2 had no effect on the timing of mitotic entry, G2 checkpoint response, or checkpoint recovery.

3.8. Cdc25a, Cdc25b, and Cdc25c depletion

G2 progression and mitotic entry depend on the ability of the Cdc25 family of protein phosphatases to activate MPF (Hutchins and Clarke, 2004; Niida and Nakanishi, 2006). To test this in the model, a series of simulations were conducted to examine the effects of separately depleting Cdc25a, Cdc25b, and Cdc25c to 0%, 1%, or 10% of baseline (Fig. S3). Depletion of Cdc25a produced a modest delay of 48 min for entry into mitosis and less than a 15 min delay in recovery from DNA damage. The Cdc25b depletion showed essentially no delay in normal mitotic entry as compared to the baseline case while adding 1.5 h to 2 h to the recovery from the damage. Like Cdc25b, depletion of Cdc25c had little effect on mitotic entry in undamaged cells. However, cells lacking Cdc25c were delayed in recovery from damage by delayed 2–2.5 h as compared to the base model.

4. Discussion

The computational model was constructed by assembling the protein–protein interactions known to play a role in the G2 to M transition or the DNA damage G2 checkpoint. This predictive mathematical model of the events involved in the progression of cells from the G2 phase to mitosis was created using the BioNetGen rule-based modeling software (Blinov et al., 2004). This model differs in several important aspects from previously published models of the cell cycle (Aguda, 1999; Kaufmann et al., 2008; Novak et al., 1998, 2007; Tyson and Novak, 2008). One is size: the Aguda model of the DNA damage G2 checkpoint consisted of 14 differential equations and the Tyson lab model of the entire cell cycle included 22 differential equations. The model described in this study consists of 769 differential equations representing nearly 2500 reactions. This increase in model complexity enabled a more detailed examination of observed behavior such as the bistable switch formed by the mutual activation of MPF and Cdc25b/c and the mutual inhibition of MPF and Wee1/pkMyt1. Another major difference is dividing the cell into cytoplasmic and nuclear compartments, in order to investigate the contribution of subcellular location and dynamics of movement between the nucleus and cytoplasm to the G2 to M transition and checkpoint response. The protein interactions in this study were modeled on the molecular level (i.e., the model consists of proteins being phosphorylated or dephosphorylated in chemical reactions and their behavior changing appropriately in response). This allowed the building of the model out of the interactions that are thought to play a role in this system as reported in the literature. Building the model in this fashion allowed simulations to be devised to determine if the interactions in the literature are sufficient to explain the observed behavior of the system. If a behavior observed experimentally is not exhibited by the model, then hypotheses about interactions that could allow the system to accurately reflect the experimental results can be rapidly simulated via the model.

There are several possible ways to extend this model, based on the new experimental evidences and hypotheses. Including the pathways that mediate the G2 checkpoint arrest in response to DNA damage will improve the type of hypothesis testing described above as well as allow for the simulation of experiments on this signaling pathway. The further division of the nuclear and cytoplasmic compartments into sub-compartments such as the Golgi complex, centrosome, nucleolus, and chromatin can better illuminate the effect of intracellular transport and the localization of proteins on the functioning of this system.

By extensively validating our model against both published and experimental results, we have been able to achieve results that are consistent with biological data. The model data reproduces the effects of depletion of pkMyt1 or Wee1 on the G2 to M transition and on the DNA damage-induced G2 checkpoint response. This result is also seen in the model output. Since the model tracks the individual proteins by amount, modification, and location, we were able to make a prediction that depletion of pkMyt1 would result in accumulation of inactive MPF in the nucleus of cells experiencing a constant DNA damage signal. An experiment conducted on mouse tumor cells found MPF present in the nucleus of pkMyt1-depleted cells that were experiencing a G2 damage arrest (Touny and Banerjee, 2006). This accumulation of nuclear MPF in pkMyt1-depleted cells may be responsible for the increased rate of mitotic entry seen in these cells. However, and more importantly, these results, if confirmed, suggest that there are one or more aspects of the intracellular trafficking of MPF that are not known. While some of the simulations regarding the role of Plk1 in the G2 to M transition and the recovery from damage arrest agree with experimental results, the model lacks some of the nuanced behavior reported in the literature. This suggests that the regulation and action of Plk1 as modeled are incomplete. The inclusion of the damage response pathways, the Aurora and Bora kinases and their regulatory effects on Plk1 as well as the added compartments can verify whether these additional factors allow the model to reproduce the entire range of behaviors seen experimentally. Similarly, model simulations show that varying the concentrations of Chk1 dramatically affected the DNA damage induced G2 arrest. Thus, adding the signaling pathways involving ATR and ATM, which activate in response to DNA damage and result in the activation of Chk1 and Chk2, can produce a more realistic simulation of the DNA damage G2 checkpoint.

5. Conclusions

The model accurately reflects experimental behavior in a substantial portion of the simulations that were conducted, demonstrating that these behaviors may be explained via the interactions included in this model. Conversely, the simulations that do not agree with experimental results indicate where interactions not currently included in the model must play a role in shaping the behavior of the DNA damage G2 checkpoint. Additionally, the model has proved capable of generating hypotheses that may be tested experimentally, demonstrating its utility in guiding experimental studies.

Acknowledgements

Supported in part by URC grant #3–10108 and PHS grants ES014635, CA16086, ES10126, and ES07017.

MLB was in part supported by NIH R01 GM095485.

The authors would like to thank Baltazar Aguda for useful conversations.

Appendix A. Supporting information

Supplementary data associated with this article can be found in the online version at http://dx.doi.org/10.1016/j.jtbi.2012.12.011.

References

Abraham, R.T., 2001. Cell cycle checkpoint signaling through the ATM and ATR kinases. Genes Dev. 15, 2177–2196.

Aguda, B.D., 1999. A quantitative analysis of the kinetics of the G(2) DNA damage checkpoint system. Proc. Nat. Acad. Sci. U.S.A. 96, 11352–11357.

Blinov, M.L., Faeder, J.R., Goldstein, B., Hlavacek, W.S., 2004. BioNetGen: software for rule-based modeling of signal transduction based on the interactions of molecular domains. Bioinformatics 20, 3289–3291.

Chylek, L.A., Hu, B., Blinov, M.L., Emonet, T., Faeder, J.R., Goldstein, B., Gutenkunst, R.N., Haugh, J.M., Lipniacki, T., Posner, R.G., Yang, J., Hlavacek, W.S., 2011. Guidelines for visualizing and annotating rule-based models. Mol. Biosyst. 7, 2779–2795.

Colvin, J., Monine, M.I., Faeder, J.R., Hlavacek, W.S., Von Hoff, D.D., Posner, R.G., 2009. Simulation of large-scale rule-based models. Bioinformatics 25, 910–917.

Doherty, S.C., McKeown, S.R., McKelvey-Martin, V., Downes, C.S., Atala, A., Yoo, J.J., Simpson, D.A., Kaufmann, W.K., 2003. Cell cycle checkpoint function in bladder cancer. J. Natl. Cancer Inst. 95, 1859–1868.

Faeder, J.R., Blinov, M.L., Hlavacek, W.S., 2009. Rule-based modeling of biochemical systems with BioNetGen. Methods Mol. Biol. 500, 113–167.

Gerard, C., Goldbeter, A., 2009. Temporal self-organization of the cyclin/Cdk network driving the mammalian cell cycle. Proc. Nat. Acad. Sci. U.S.A. 106, 21643–21648.

Harper, J.W., Elledge, S.J., 2007. The DNA damage response: ten years after. Mol. Cell 28, 739–745.

Hartwell, L.H., Kastan, M.B., 1994. Cell cycle control and cancer. [Review] [101 refs]. Science 266, 1821–1828.

Hirai, H., Iwasawa, Y., Okada, M., Arai, T., Nishibata, T., Kobayashi, M., Kimura, T., Kaneko, N., Ohtani, J., Yamanaka, K., Itadani, H., Takahashi-Suzuki, I., Fukasawa, K., Oki, H., Nambu, T., Jiang, J., Sakai, T., Arakawa, H., Sakamoto, T., Sagara, T., Yoshizumi, T., Mizuarai, S., Kotani, H., 2009. Small-molecule inhibition of Wee1 kinase by MK-1775 selectively sensitizes p53-deficient tumor cells to DNA-damaging agents. Mol. Cancer Ther. 8, 2992–3000.

Hlavacek, W.S., Faeder, J.R., Blinov, M.L., Posner, R.G., Hucka, M., Fontana, W., 2006. Rules for modeling signal-transduction systems. Sci. STKE, 2006, re6.

Hutchins, J.R., Clarke, P.R., 2004. Many fingers on the mitotic trigger: post-translational regulation of the Cdc25C phosphatase. Cell Cycle 3, 41–45.

Juan, G., Traganos, F., James, W.M., Ray, J.M., Roberge, M., Sauve, D.M., Anderson, H., Darzynkiewicz, Z., 1998. Histone H3 phosphorylation and expression of cyclins A and B1 measured in individual cells during their progression through G2 and mitosis. Cytometry 32, 71–77.

Kaufmann, W.K., Nevis, K.R., Qu, P., Ibrahim, J.G., Zhou, T., Zhou, Y., Simpson, D.A., Helms-Deaton, J., Cordeiro-Stone, M., Moore, D.T., Thomas, N.E., Hao, H., Liu, Z., Shields, J.M., Scott, G.A., Sharpless, N.E., 2008. Defective cell cycle checkpoint functions in melanoma are associated with altered patterns of gene expression. J. Invest. Dermatol. 128, 175–187.

Niida, H., Nakanishi, M., 2006. DNA damage checkpoints in mammals. Mutagenesis 21, 3–9.

Nilsson, I., Hoffmann, I., 2000. Cell cycle regulation by the Cdc25 phosphatase family. Prog. Cell Cycle Res. 4, 107–114.

Novak, B., Tyson, J.J., Gyorffy, B., Csikasz-Nagy, A., 2007. Irreversible cell-cycle transitions are due to systems-level feedback. Nat. Cell Biol. 9, 724–728.

Novak, B., Kapuy, O., Domingo-Sananes, M.R., Tyson, J.J., 2010. Regulated protein kinases and phosphatases in cell cycle decisions. Curr. Opin. Cell Biol..

Novak, B., Csikasz-Nagy, A., Gyorffy, B., Chen, K., Tyson, J.J., 1998. Mathematical model of the fission yeast cell cycle with checkpoint controls at the G1/S, G2/M and metaphase/anaphase transitions. Biophys. Chem. 72, 185–200.

Pomerening, J.R., Sontag, E.D., Ferrell Jr., J.E., 2003. Building a cell cycle oscillator: hysteresis and bistability in the activation of Cdc2. Nat. Cell Biol. 5, 346–351.

Qu, Z., Weiss, J.N., MacLellan, W.R., 2003. Regulation of the mammalian cell cycle: a model of the G1-to-S transition. Am. J. Physiol. Cell Physiol. 284, C349–C364.

Rieder, C.L., 2011. Mitosis in vertebrates: the G2/M and M/A transitions and their associated checkpoints. Chromosome Res.: Int. J. Mol., Supramol. Evol. Aspects Chromosome Biol. 19, 291–306.

Sha, W., Moore, J., Chen, K., Lassaletta, A.D., Yi, C.S., Tyson, J.J., Sible, J.C., 2003. Hysteresis drives cell-cycle transitions in Xenopus laevis egg extracts. Proc. Nat. Acad. Sci. U.S.A. 100, 975–980.

Smits, V.A., Klompmaker, R., Arnaud, L., Rijksen, G., Nigg, E.A., Medema, R.H., 2000. Polo-like kinase-1 is a target of the DNA damage checkpoint. Nat. Cell Biol. 2, 672–676.

Stark, G.R., Taylor, W.R., 2006. Control of the G2/M transition. Mol. Biotechnol. 32, 227–248.

Takai, N., Hamanaka, R., Yoshimatsu, J., Miyakawa, I., 2005. Polo-like kinases (Plks) and cancer. Oncogene 24, 287–291.

Touny, L.H., Banerjee, P.P., 2006. Identification of both Myt-1 and Wee-1 as necessary mediators of the p21-independent inactivation of the cdc-2/cyclin B1 complex and growth inhibition of TRAMP cancer cells by genistein. Prostate 66, 1542–1555.

Toyoshima-Morimoto, F., Taniguchi, E., Nishida, E., 2002. Plk1 promotes nuclear translocation of human Cdc25C during prophase. EMBO Rep. 3, 341–348.

Tyson, J.J., Novak, B., 2008. Temporal organization of the cell cycle. Curr. Biol. 18, R759–R768.

Tyson, J.J., Baumann, W.T., Chen, C., Verdugo, A., Tavassoly, I., Wang, Y., Weiner, L.M., Clarke, R., 2011. Dynamic modelling of oestrogen signalling and cell fate in breast cancer cells. Nat. Rev. Cancer 11, 523–532.

Unsal-Kacmaz, K., Mullen, T.E., Kaufmann, W.K., Sancar, A., 2005. Coupling of human circadian and cell cycles by the timeless protein. Mol. Cell. Biol. 25, 3109–3116.

van Vugt, M.A., Medema, R.H., 2005. Getting in and out of mitosis with Polo-like kinase-1. Oncogene 24, 2844–2859.

van Vugt, M.A., Yaffe, M.B., 2010. Cell cycle re-entry mechanisms after DNA damage checkpoints: Giving it some gas to shut off the breaks!. Cell Cycle 9, 2097–2101.

van Vugt, M.A., Gardino, A.K., Linding, R., Ostheimer, G.J., Reinhardt, H.C., Ong, S.E., Tan, C.S., Miao, H., Keezer, S.M., Li, J., Pawson, T., Lewis, T.A., Carr, S.A., Smerdon, S.J., Brummelkamp, T.R., Yaffe, M.B., 2010. A mitotic phosphorylation feedback network connects Cdk1, Plk1, 53BP1, and Chk2 to inactivate the G(2)/M DNA damage checkpoint. PLoS Biol. 8, e1000287.

Wang, Y., Decker, S.J., Sebolt-Leopold, J., 2004. Knockdown of Chk1, Wee1 and Myt1 by RNA interference abrogates G2 checkpoint and induces apoptosis. Cancer Biol. Ther. 3, 305–313.

Wells, N.J., Watanabe, N., Tokusumi, T., Jiang, W., Verdecia, M.A., Hunter, T., 1999. The C-terminal domain of the Cdc2 inhibitory kinase Myt1 interacts with Cdc2 complexes and is required for inhibition of G(2)/M progression. J. Cell Sci. 112, 3361–3371, Pt 19.

Yang, L., Han, Z., Robb MacLellan, W., Weiss, J.N., Qu, Z., 2006. Linking cell division to cell growth in a spatiotemporal model of the cell cycle. J. Theor. Biol. 241, 120–133.